International Journal of Hydrogen Energy 120 (2025) 385–392

Contents lists available at ScienceDirect

International Journal of Hydrogen Energy

journal homepage: www.elsevier.com/locate/he

Evaluation of simplified test rig for high throughput screening of proton exchange membrane water electrolysis components

Florian Berg, Meital Shviro [1], Marcelo Carmo [2], Nikolai Utsch, Martin Müller [*]

Forschungszentrum Jülich GmbH, Institute of Energy Technologies, IET-4: Electrochemical Process Engineering, 52425, Juelich, Germany

ARTICLE INFO

Handling editor: Umit Demirci

ABSTRACT

The research and development of components for polymer electrolyte membrane (PEM) water electrolysis are often constrained by limited test rig capacity. This study introduces a novel, compact test rig to facilitate rapid screening and extended operation of mini cells, featuring an active area of just 1.13 cm^2. The setup can simultaneously evaluate the performance of 24 test cells, offering a simple, cost-effective, and space-saving solution. Utilizing hydrostatic pressure, the system operates without an active water supply, significantly reducing the costs and materials required for components such as porous transport layers and membrane electrode assemblies. This innovative test rig accelerates material characterization for PEM electrolyzers and supports comprehensive long-term operation studies, thereby advancing the field of electrolysis research.

1. Introduction

Hydrogen is an indispensable substance for industry and has exceptional importance as a large-scale energy storage in future carbon-free energy systems. Using electricity, especially from renewable energy sources, hydrogen and oxygen can be produced, for example by polymer electrolyte membrane water electrolysis (PEM-WE) [1–3]. Due to the corrosive environment of the acidic membrane and oxidative conditions on the anode the cell components often are constructed by titanium [4]. As anode current collector, typically titanium-based porous transport layers (PTLs) such as sintered discs, foams, felts, or meshes are used which are coated with platinum, gold, or iridium to overcome titanium passivation, while a carbon-based gas diffusion layer (GDL) on the cathode is used [5–9]. In addition, costly platinum group metals (PGMs) are required as catalysts for the hydrogen evolution reaction (HER) and oxygen evolution reaction (OER) and there has been much effort to develop highly active OER catalysts to decrease or eliminate Ir loading. However, the development of such new OER catalysts requires fast and reliable screening methods to identify promising materials within a reasonable time scale. Typically, rotating disk electrode (RDE) measurements are performed in a three-electrode cell because only a few milligrams of catalyst are needed to assess the OER activity as well as the catalyst stability. Although it is well established that there is a discrepancy between a catalyst lifetime obtained from RDE and PEM-WE under similar operating conditions. Consequently, accelerated stress tests (AST) on the membrane electrode assembly (MEA) level are required to evaluate catalyst stability at realistic operating conditions [9–13]. However, a key challenge in these studies is the lack of statistical robustness, as single-cell testing limits the number of samples that can be characterized under identical conditions. To address this limitation, we introduce a novel high-throughput test rig capable of simultaneously monitoring 24 mini PEM-WE cells, significantly improving the reliability and statistical evaluation of long-term characterization studies. To assess extended stability runtimes up to 5000 h are used in academic research [14].

Whereas the common active electrode size in the laboratory is in the range of 5–100 cm^2, an upscaling of the water-splitting process is necessary for industrial processes, but for research and development (R&D) a reduced cell size has some advantages such as more compactly [4,15]. It also reduces the amount of expensive PGMs such as platinum, iridium, and newly developed catalysts, as well as the cost of PTLs and their protective coatings thereby reducing the overall research costs [8]. Besides, the amount of newly developed materials in the laboratory is often limited and therefore a smaller cell size can open the way for long-term catalyst durability and activity testing in real PEM-WE systems [10].

* Corresponding author.
E-mail address: mar.mueller@fz-juelich.de (M. Müller).
[1] Current address: Chemistry and Nanoscience Center, National Renewable Energy Laboratory (NREL), Golden, CO, 80401 USA.
[2] Current address: Nel Hydrogen, 10 Technology Drive, Wallingford, CT 06492, USA.

https://doi.org/10.1016/j.ijhydene.2025.03.210
Received 23 November 2024; Received in revised form 12 March 2025; Accepted 13 March 2025
Available online 26 March 2025

Furthermore, to improve the economics of PEM electrolyzers and reduce the cost in general, developments not only in catalyst materials but also in various components in the field of MEAs and PTLs are crucial [2,4,16]. However, the test capacity of single test cell characterization is limited by the availability of test stations that provide the necessary peripherals to drive an electrolysis cell and generate record measurement results. Commercially available test rigs for cell testing have large peripherals, require a lot of space, and are expensive, mainly because of their ability to operate under high-pressure conditions. This means that there is a large volume of pressurized hydrogen in the media chambers, particularly on the cathode side. As this volume contains a large amount of energy, the containers and sensors must be designed to be correspondingly safe to ensure safe operation in the event of possible defects. This leads to high costs and complex safety protocols. The new test stand presented here, which is initially operated without pressure, can also be operated safely under pressure with significantly less effort due to its limited volume. In addition, the cells used in conventional test stands (usually only one) must be individually temperature-controlled, which requires a great deal of effort in terms of control and heating technology. The supply lines to the cells must also be thermally insulated and the media may need to be preheated. These are expenses that make test stands complex and expensive. In addition, long-term stability studies of cell components are important to understand degradation processes [17, 18] and this could tie up test rigs for weeks or months, slowing down research efforts. To address these challenges, we have introduced a compact test rig that significantly improves the efficiency of evaluating PEM components. Unlike traditional setups that yield a single data point per test cell, this new rig can simultaneously test 24 cells, generating a comprehensive dataset within the same timeframe. This increased data volume enhances the ability to use machine learning and artificial intelligence for pattern recognition, material optimization, and accelerated development of more effective PEM electrolyzers. By expanding the dataset, the rig facilitates more robust predictive models and insights, driving innovation and progress in electrolysis research.

In this work, we introduce our novel high-throughput test rig capable of simultaneously evaluating 24 individual PEM-WE mini-cells under realistic operating conditions. Compared with existing test systems it provides the following advantages.

1. Enables parallel testing of 24 individual cells, significantly reducing characterization time and improving statistical analysis.
2. Maintains reproducibility by ensuring identical test conditions across multiple samples.
3. Bridges the gap between fundamental research and industrial applications by offering a scalable platform adaptable to larger cell sizes.

This compact and cost-effective system is designed to streamline the screening of key electrolyzer components, including PTLs and MEAs incorporating different catalysts. With a reduced active area of 1.13 cm^2 per cell, our setup significantly minimizes material consumption while enabling both short-term performance assessments and long-term stability studies. By operating multiple cells in parallel, the test rig enhances statistical reliability and accelerates the research process compared to conventional single-cell test stations. We present initial measurements under full capacity, assess the system's limitations, and propose future improvements to further expand its applicability.

2. Setup

2.1. Mini test cell

Miniature PEM electrolytic cells (mini-cells) with an active area of 1.13 cm^2 were used for electrochemical characterization. Lohoff et al. presented a first mini-cell design in 2016 [19], based on this first generation further improvement has been done and referred to here as generation II (Fig. 1a). The generation II cells consist of two flanges made of titanium to minimize contact resistance. To achieve greater flexibility in the use of different PTL thicknesses and easier handling during disassembly or assembly, three 35 mm long stainless-steel tie rods to compress the cell replaced the clamping ring. The use of flat gaskets eliminated the need for the O-ring seal (Gen I) cutouts. Two 4 mm diameter polypropylene pins adjust the cell components during assembly. The anodic and cathodic flanges have different designs: the cathodic flange has a flat surface, 18 holes with a diameter of 1.3 mm, and a circular arrangement that allows the discharge of hydrogen and entrained water. The thickness of the cathodic GDL is freely selectable and adjustable by varying the thickness of the flat gasket such as cloths or carbon paper can be used. The anode side has only one opening with a required diameter of 10 mm as the cell design is based on anodic water supply by a hydrostatic configuration without pumps. If the opening were smaller, the water supply would not be guaranteed, as the water could not reach the PTL while oxygen gas rises in the opposite direction. In addition, there is a 0.4 mm deep notch with a diameter of 12 mm, which allows PTLs thicker than 400 µm to be inserted and retained. Because the PTL only rests on the edges, only tough and stable PTLs are useable. Otherwise, the PTL bends due to the missing stabilization and the contact with the MEA decreases. When inserting PTLs with higher thickness, the resulting gap gets closed by using PTFE gaskets. The flanges are equipped with inner threads which allows to use of different fittings. In this work, stainless steel fittings were chosen to insert the cell into the test rig. A small unintentional gap between the fitting and the anodic flange was closed with a porous titanium ring. The surface of both flanges is platinized to minimize degradation. The cells had 4 mm current connections, 2 mm voltage sensing connections, and heater cartridge connections. The latter are provided only in case experiments are performed outside the test rig.

2.2. Test rig

The miniature test cells were characterized in an in-house multiple single-cell test rig. Due to the small cell design and the test rig concept, it is possible to characterize 24 mini cells simultaneously. The concept is kept as simple as possible and works without active water flow, only the anode is supplied with water according to hydrostatic rules. Compared to conventional test stands, the design of the test stand can be significantly simplified. In addition to a reduction in costs, reliability can also be increased with a reduced number of components, as fewer subcomponents run the risk of failing. A rough calculation of the number of components is given in Table 1. It clearly shows the simplification of the presented test station. In the case of the 24 cells high throughput setup 34 complex components needed, compared to 24 single cell test stations were 192–240 complex components needed. The variation of the number of components depends on the operation strategy with or without cathodic media supply. A direct measure of the complexity is the number of "complex components per cell" and here we achieve a value far below 2.

A container (upper water storage) filled with water supplies the entire anode circuit. A schematic of the test rig is shown in Fig. 2a. The main core is formed by a climate chamber (MK 720, Binder) with an internal volume of 0.73 m^3. The theoretical temperature range for climate chambers range from −40 °C to +180 °C. However, the practical upper limit is approximately 90 °C, primarily due to the long-term thermal stability requirements of materials such as polymers, insulation materials, and sealing agents used within the chamber. Exceeding this temperature can significantly reduce the lifespan and reliability of these materials [20,21]. Operating at or below 90 °C ensures material durability and consistent performance over extended testing periods.

The mini cells are integrated along the periphery within the climate chamber, ensuring constant ambient conditions for the electrochemical characterization. This controlled environment facilitates the rapid and reproducible simulation of stress factors such as temperature variations.

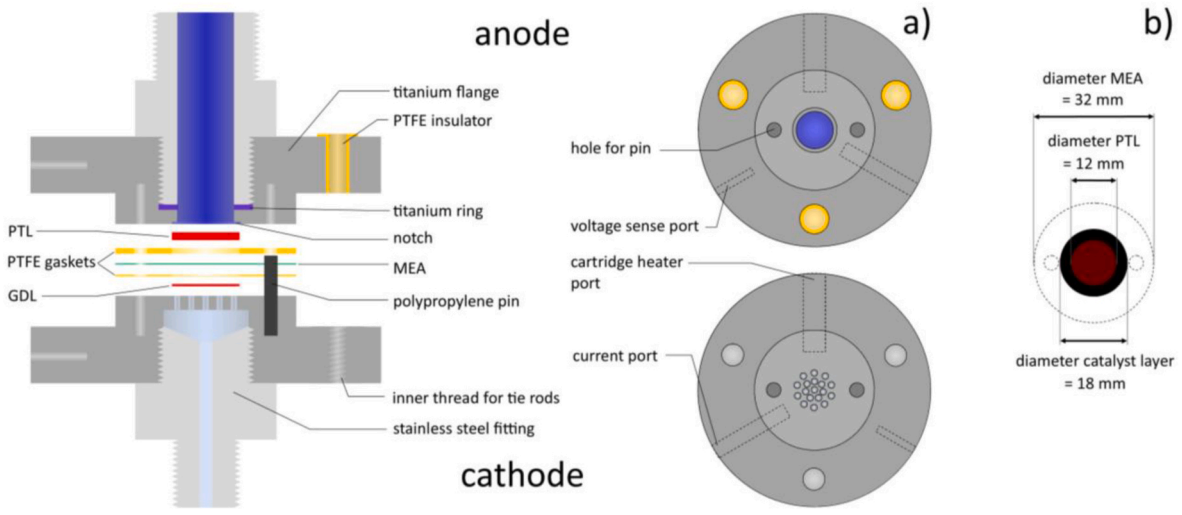

Fig. 1. – Scheme of a mini-cell generation II and its components: a) left: cross section of the components and assembling process, right: top view of the cell flanges; b) size ratio of MEA and PTL. Abbreviations: membrane electrode assembly MEA, porous transport layer PTL, gas diffusion layer GDL, polytetrafluorethylene PTFE.

Table 1
Estimation of the number of important components for different test stand configurations. Cables and insulation materials were neglected due to the relatively low costs.

Component	Single cell setup	24 cells in single cell setup	24 cells in high throughput setup
Cells (Sub-elements are not considered)	1	24	24
Preheater anode	1	24	0
Preheater cathode	0, 1	0, 24	0
Gas separator anode	1	24	1
Gas separator cathode	1	24	1
Circulation pump anode	1	24	0
Circulation pump cathode	0, 1	0, 24	0
Power supply cell	1	24	6
Gas sensor (H_2 in O_2)	1	24	1
Heater control system with thermocouples	1	24	0
Climate chamber	0	0	1
Number of complex components	**8–10**	**192–240**	**34**
Complex components per test cell	~9	~9	~1.42

The inner periphery - tubes, pipes, and valves - is mounted on an aluminium framework, which provides mechanical stability and uniform exposure to induced stresses. In this configuration, four cells are connected in series to the water supply, allowing for continuous monitoring and evaluation of stress responses under accelerated conditions. Four cells were connected in series to one water supply. This serial grouping is repeated six times (dashed lines in Fig. 2a). Fig. 2d shows the setup more clearly. The six repeating units are arranged in two levels and three rows, making the total number of cell units 24.

In electrolysis, bubbles of oxygen gas rise at the anode through the water supply line. This anodic system consists of several parts.

1) the horizontal anode centreline is a glass cylinder 4 cm in diameter and 80 cm in length. It has a slope of 4° to remove the oxygen gas.
2) the vertical anode tubes have an inner diameter of 10 mm, which cannot be smaller since the concept will not work as the gas produced will displace the water.

To measure fewer than 24 cells, each cell needs to be shut down using valves on the anodic and cathodic sides. The anode tubes with a 10 mm inner diameter have bulky commercially available valves, for this reason, a silicone tube was used to connect the glass cylinder and PTFE tube. The glass cylinder in the climate chamber is connected to a mixing chamber by PTFE tubes with a 10 mm inner diameter. The mixing chamber, a glass cylinder with a diameter of 9 cm, is where the anodic product gas from all six rows of cells converges. Due to hydrostatic buoyancy, the gas rises to the top and is separated from the liquid phase. The vapor condenses, and the liquid water is collected in the lower water reservoir.

The cathodic system comprises PTFE tubes with an inner diameter of 4 mm connected with stainless steel fittings. Ball valves in the system enable the use of a variable number of mini cells. Additional ball valves are installed to block an entire circuit of four cells when not in use to minimize the total cathodic volume. Water that enters the membrane due to electroosmotic resistance is expelled by the generated gas. After gas separation, the hydrogen is removed by the exhaust system, and the water carried along in the cathode circuit is discharged into the wastewater.

Six power supplies (HMP4040, Rhode & Schwarz), each with four separate channels, were used for electrochemical cell characterization. Each channel can reach a maximum current of 10 A, and the maximum output power per channel is 160 W. A self-programmed LabVIEW software controls the power supplies. A four-wire measurement setup with separate voltage measurement leads is used for characterization. Each cell got one pair of 1 mm^2 silicone covered measuring leads with a 4 mm connector and the voltage sense lines have a cross-section of 0.5 mm^2 with a 2 mm connector. In addition, the temperature of a random mini-cell and a point in the middle of the chamber is recorded using thermocouples and a data acquisition system (TC-08, Omega).

The lower 5 L water storage tank is fed by an upper 60 L water storage tank located 1.5 m above it and refilled manually. Thus, potential energy is the driving force for automatic water refilling and is controlled by two capacitive sensors (BC10-QF5.5-AP6X2, Turck) and a magnetic valve. Due to the constant water level in the lower water reservoir, the hydrostatic pressure in the entire anodizing system is constant. However, if there is no further water supply and the water level drops, additional sensors detect this, and the power supply is switched off. Because of the small cell size, the amount of hydrogen is easily manageable. The total hydrogen production rate of 24 cells at a current of 3 A cm^{-2} is about 43 L h^{-1}. The volume of the cathode tube is minimized, and the hydrogen is fed into the exhaust system. There is no control over the hydrogen transfer on the anodic side. Since the anodic system is surrounded by water, the total volume is small, and the product gas is exhausted by the fastest route. The case would be more

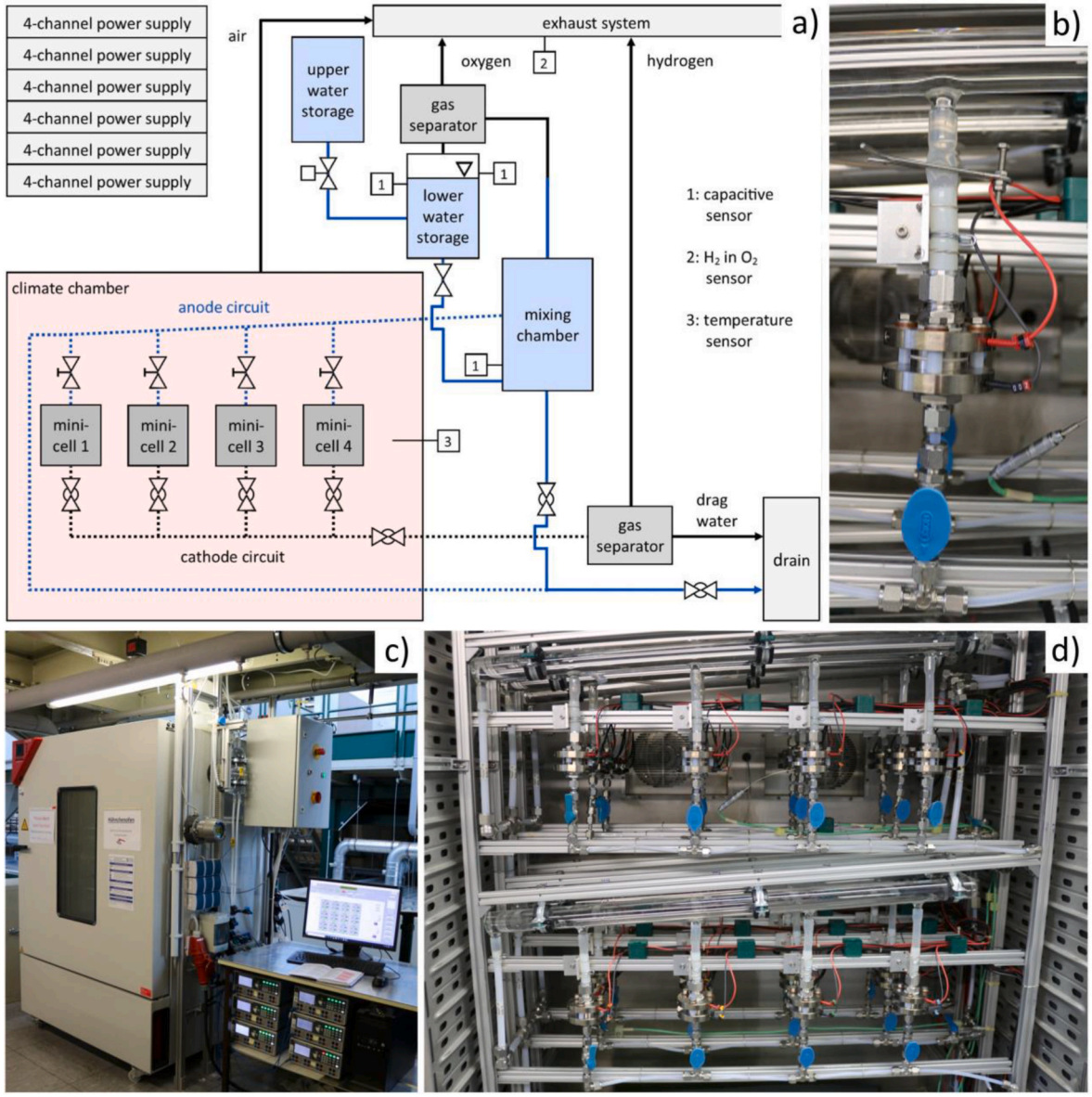

Fig. 2. – Multiple single-cell test rig for mini-cell characterization: a) scheme of test rig; b) cell unit with closed anodic 'valve'; c) whole test rig setup with climate chamber, power supplies, exhaust system, safety control unit, lower water storage and outer periphery; d) setup inside climate chamber with built-in 24 mini-cells.

critical if leaks occurred at some connection fittings in the climate chamber and hydrogen was released. To detect this, the chamber is connected to the exhaust system and monitored by a hydrogen gas sensor (Polytron SE Ex PR M1 DD, Dräger). If a limit of 2 % hydrogen in oxygen (half the lower explosion limit) is exceeded, the chamber and power supplies automatically shut down.

3. Experimental

3.1. MEA preparation

The in-house electrode fabrication starts from solvent-based catalyst inks with a coating process via doctor-blade techniques and decal transfer method for the fabrication of Nafion® 117 MEAs with a catalyst area of 2.54 cm^2 [17]. As the anode catalyst IrO_2 (Alfa Aesar, Premion, 99.99 %) was used and 60 % Pt/C (HiSPEC 9100, Johnson & Matthey) as cathode catalyst. To prepare the anode catalyst ink, the catalyst powder and the aqueous ionomer solution (10 % Nafion®) were dispersed with appropriate additives in total volumes of 10 mL and agitated for 4 min in an ultrasonic homogenizer. For the cathode catalyst ink, the catalyst powder and alcoholic ionomer solution (15 % Nafion®) were dispersed with 2-propanol and 2-butanol in a total volume of 20 mL. The inks were then coated onto inert decal substrates by automated bar coating (Coatmaster 509 MCI, Erichsen GmbH & Co. KG) and the dried electrode layers were hot-pressed onto the cleaned Nafion® membrane at a temperature of 130 °C and 2.6 kN cm^{-2} for about 3 min. The final catalyst loadings were 2.17 ± 0.22 mg cm^{-2} IrO_2 and 0.87 ± 0.19 mg cm^{-2} Pt.

In the CCM preparation technique described here, the focus is on achieving reproducible production to ensure the incorporation of identical CCMs into each cell. However, this setup can also be utilized to compare a large number of samples extracted from different locations of a large-scale produced CCM enabling the assessment of spatial variations. Such manufacturing inconsistencies have been previously reported by Burdzik et al. [22].

3.2. PTL preparation

As GDL on cathode side carbon paper (TGP-H 120, Toray) was used

and porous titanium sinter plates (SIKA-T 10, GKN) on anode will be referred to hereinafter as Ti-PTLs. While the round carbon paper with a 350 μm thickness and diameter of 12.0 mm was prepared by punching out with a cutting die and a press, the round Ti-PTLs with a thickness of 1.4 ± 0.1 mm and diameter of 12.0 mm were manufactured by laser cutting. This process has created a grid at the bottom of the PTL that was removed by manual polishing with a grindstone (bench stone original-Arkansas, Hoffmann Group). Polishing was carefully performed by moving the sample in a figure-eight motion. The surface roughness of the sample was analyzed before and after polishing using a non-contact profilometer (CT-300, cyberTECHNOLOGIES GmbH) with a lateral resolution of 0.05 μm and a step size of 5 μm. Polishing had no measurable effect on the surface roughness, as the average arithmetic height changed from 10.9 ± 1.3 μm before polishing to 11.2 ± 1.6 μm after polishing.

To remove contaminants and organic substances caused by the grinding process the Ti-PTLs were cleaned by a procedure described by Liu et al. [7]. First, the PTLs were soaked in 80 °C hot Milli-Q water for 15 min, then immersed in 2-propanol and acetone for 15 min each in an ultrasonic bath (ultrasonic cleaner USC200T, VWR), followed by two 15-min immersions in 80 °C water. The PTLs were air-dried overnight at 60 °C and then coated with platinum (Pt 99.95 % target, MaTeck) on both sides using a PVD unit (Sputter Coater Q150T ES, Quorum Technologies) at 30 mA for 360 s to ensure long-term stability.

3.3. Test cell assembling

24 mini cells were assembled with MEAs of the same batch. The Ti-PTL was inserted in the nut of the anodic flange with a polished side looking up to the MEA. By varying the gasket thickness and adjusting the torque range from 0.5 to 5 Nm, the optimal tie rod compression was determined using two different pressure-sensitive films (Prescale, Fuji Film CMV Hoven GmbH) with a pressure range of 0.2 MPa–2.5 MPa. The final procedure involved tightening the three tie rods in two stages, first to 0.35 Nm and then to 0.5 Nm, to ensure homogeneous torque application and minimize the possibility of PTL-MEA contact issues. Toray® paper was used as the cathodic GDL and sealed with a 300 ± 5 μm thick PTFE flat gasket. The platinum-coated Ti-PTL on the anode was sealed with a 1000 ± 5 μm thick PTFE gasket. Although the catalyst layer of the MEAs is 2.54 cm^2, the overall active area of the cells is limited by the 1.13 cm^2 current collectors, and the sealing used (see Fig. 1b). Along with the PTL treatment discussed above, this methodology effectively minimized cell-to-cell variability arising from component fluctuations.

3.4. Electrochemical characterization

The 24 test cells were built in the mini-cell PEM-electrolysis test rig. The temperature of the climate chamber was set at 80 °C for about 3 h. After this time the temperature of the air and cells was constant, and the activation was started. The activation protocol employed in this study aligns with established practices in electrochemical cell conditioning. Initially, a current density of 0.2 A cm^{-2} was applied for 30 min in galvanostatic mode to condition the membranes and catalyst layers gently. Subsequently, the current density was increased to 1 A cm^{-2} for 30 min to further enhance the activation process and improve interfacial contact between components. Following the galvanostatic steps, the system was operated in potentiostatic mode at a constant potential of 1.7 V for 7 h. This approach ensures complete activation of the cell components and stabilization of the catalytic activity, preparing the cells for reliable performance evaluation. Similar potentiostatic activation methods have been documented in previous studies [23]. The activation was followed by a performance evaluation, conducting current controlled VI-curves using 5-min steps.

The maximum potential was set on 2 V and the current density was increased in the following increments: open circuit, 10 mA cm^{-2}, 25 mA cm^{-2} to 125 mA cm^{-2} with Δ25 mA cm^{-2}, 250 mA cm^{-2} to 2000 mA cm^{-2} with Δ250 mA cm^{-2} and 2500 mA cm^{-2} to 4000 mA cm^{-2} with Δ500 mA cm^{-2}. After this first polarization measurement, a second high-to-low current density curve was started with a reversed order from 4.000 A cm^{-2} to 0.01 A cm^{-2} with the same increments described before.

3.5. Heat management

The heat balance of the cell plays a major role in electrochemical characterization, as the temperature has a strong effect on the cell voltages. The heat balance and the optimization of the heat balance have been extensively investigated by Scheepers [24]. Due to the passive temperature control of the test system — achieved by integrating it into a heating cabinet operating at a constant temperature — the heat transfer into the test cell is inherently limited due to the low heat transfer coefficient between air and cell components, which results in reduced thermal exchange at small temperature gradients. Therefore, analyzing the heat balance is particularly important, as temperature has a significant influence on electrochemical performance and polarization plot measurements. The heat and energy balance in this setup follows fundamental thermodynamic relationships: The total energy input comprises the electrical power P_{el} in kW and the enthalpy supplied by the water consumed in the reaction $\dot{m}_{H2O} c_{H2O} T$. $\dot{m}_{H2O}$ is the specific mass flow in kg s^{-1}, c_{H2O} is the heat capacity with constant 4.18 kJ kg^{-1} K^{-1} and T is the temperature in Kelvin. This energy is distributed among the energy required for water splitting (water mass flow and the reverse formation enthalpy $\dot{m}_{H2O} \Delta h_{f_{H2O}}$ with $\Delta h_{f_{H2O}}$ 15.833 MJ kg^{-1}) and the energy needed for humidification of the generated hydrogen and oxygen gases up to saturation vapor pressure. c_{H2} represents the heat capacity of the hydrogen with 14.2 kJ K^{-1}, c_{O2} represents the heat capacity of the oxygen with 0.91 kJ K^{-1}, x_{H2} is the dimensionless mass ratio of water vapor in hydrogen, x_{O2} is the dimensionless mass ratio of water vapor in oxygen and it is assumed that hydrogen and oxygen are saturated with water vapor. The following vapor pressures were used to calculate the temperature-dependent vapor content at the respective temperatures: 75 °C–39,000 Pa, 80 °C–48,040 Pa, 85 °C–58,800 Pa. r_0 is the evaporation enthalpy with 2500 kJ kg^{-1}, and c_{H2Ov} is the heat capacity of water vapor with 1.86 kJ K^{-1}. It is assumed that we have an isothermal process. For this to be the case, heat $\dot{Q}$ in kW must be supplied or dissipated across the balance limits of the system.

$$P_{el} + \dot{m}_{H2O} c_{H2O} T + \dot{m}_{H2O} \Delta h_{f_{H2O}} - \dot{m}_{H2}(c_{H2} + x_{H2}(r_0 + c_{H2O_v} T))$$

$$- \dot{m}_{O2}(c_{O2} + x_{O2}(r_0 + c_{H2O_v} T)) = -\dot{Q}$$

By applying these parameters to the current-voltage characteristics, the heat balance shown in Fig. 3 illustrates how the required thermal energy varies with temperature and electrochemical performance. A positive value for the specific heat means that a heat flow from the environment into the cell is needed and a negative value means a demand for cooling. In addition, Fig. 3 demonstrates that at 80 °C (Q_80 curve), the necessary heat supply remains relatively moderate, making this temperature range optimal for characterization. Additionally, at 1.8 V, the system reaches thermal equilibrium without needing active cooling or heating. However, when aiming for higher efficiencies — such as operating at 1.7 V — reducing the temperature to 75 °C minimizes the need for external heat input or dissipation, as reflected in the plotted heat flux trends (Q_75 heat flux at 75 °C, Q_85 heat flux at 85 °C). At ambient pressure Fig. 3 highlights the sense for conducting characterization measurements at a temperature of 80 °C, as this range corresponds to relatively moderate heat flows that need to be supplied to the test cell system.

For pressurized system characterization, additional heat dissipation is required since the proportion of heat lost through evaporative cooling decreases under elevated pressure conditions. This necessitates enhanced thermal management strategies to maintain stable operating

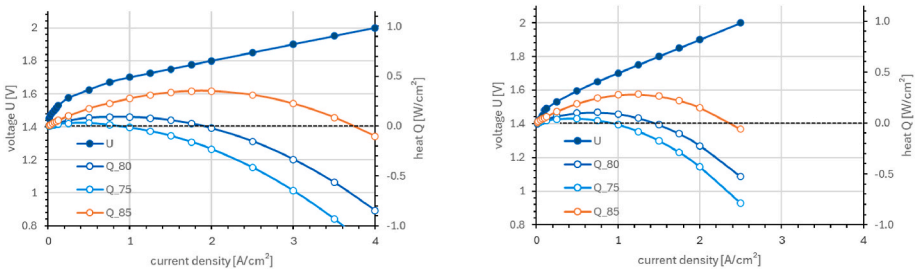

Fig. 3. – Typical polarization plot monitored in state-of-the-art PEM electrolysis cells. Necessary heat flux in relation to the active cell area and in dependency of the operating temperature (Q_80: 80 °C; Q_75: 75 °C; Q_85: 85 °C). With high performance cell (left), with conventional cell (right).

conditions. This means that the temperature in the chamber will be adjusted by consideration of heat management at a certain cell voltage and pressure level. To evaluate this, further investigations are required when recording the respective cell temperature, which would go beyond the scope of this publication and should be further elaborated in the future.

If no heat flux across the system boundaries of the cell occurs, the cell temperature is a function of the cell voltage and the operating pressure (here calculated for 1 bar, 1.5 bar, 3 bar) shown in Fig. 4. This means that if a temperature other than the one calculated is aimed, a heat flow into or out of the cell must occur. Possible additional heat inputs due to hydrogen and oxygen permeation are not considered.

4. Results and discussion

Finally, a long-term operation of approximately 22 days was initiated in potentiostatic mode at 2 V. 20 out of 24 cells have undergone this process. Four cells (cell 5 to cell 8) were not connected to any power supply. Fig. 5 presents the *in-situ* measurement results.

In Fig. 5a the temperature of the climate chamber and the cathode flange of cell 3 are plotted versus absolute time. The temperature of the chamber is precise, and we can adjust it with an accuracy of about 1 K (see Fig. 5a). According to the calculation shown in subchapter 3.5 “heat management”, an operation at 2 V means that the cells have been operated during this procedure at a local temperature of about 85 °C inside the electrochemical active layers. The increased temperature leads to a warming of the cell, that can be seen, as the cell temperature differs from the temperature of the climate chamber, and we measured 82 °C. This correlation should be considered in future measurements and the temperature of the climate chamber should be reduced by about one or 2 °C to reach an operating temperature of 80 °C in the cell body or in an ideal case the cell voltage should be decreased to 1.8 V where no heat flux is needed to reach 80 °C. Especially in long-term operation, cells

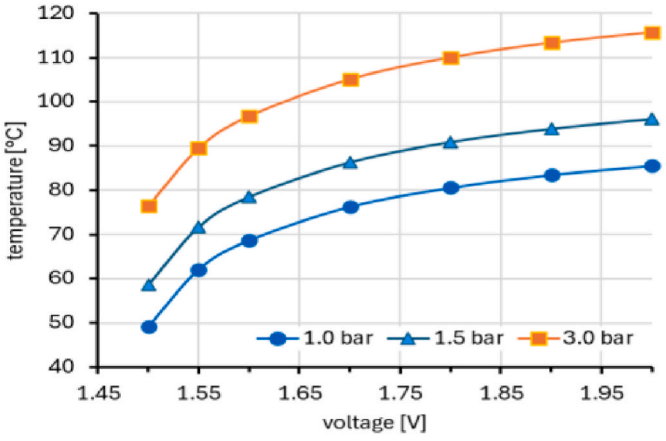

Fig. 4. – Cell temperatures as a function of the cell voltage and the set operating pressure, with equal pressure on the anode and cathode.

should be operated at operating points where no heat flow across the system boundaries occurs. The key to setting such an operating point lies in the choice of cell voltage and temperature given in Fig. 4. In this case a different cell performance has no influence on the temperature level in the cell.

While the temperature of the climate chamber is constant for a long time, the temperature of the cell depends on the applied current density and increases by 1.5 °C during the VI-curve measurement (arrows in Fig. 5a) which is in correlation with our calculation of the heat fluxes. To mitigate this effect during polarization plot monitoring, it may be beneficial to shorten the measurement duration and increase both the outer surface area and mass of the test cells. As the current density decreases during long-term operation, the temperature also decreases until the operating time of 200 h while the voltage was constant 2 V. After that, a slow temperature increase in the cell can be observed.

On the one hand, the climate chamber enables constant ambient conditions which is important because the performance evaluation is strongly dependent on temperature. But on the other hand, this potentially might be a weak point in long-term testing. If the ohmic resistance increases with time due to degradation, cell temperature will increase. Due to a missing individual active temperature control of each cell, the cell temperature will differ from the ambient conditions. The cells have an opening for an additional cartridge heater, but this supplementary temperature control would make the concept more complex and expensive.

During the activation process (Fig. 5b), the gap between the highest and the lowest current density is large at about 0.4 A cm^{-2}. The current density of cells 21, 20, 18, and 16 is not stable at the end of 8 h conditioning process. The IEA Electrolysis Annex 30 reported a round-robin test to initialize a benchmarking with a standardized working protocol [20], 1.7 V voltage-controlled was defined as the operation of cell conditioning until the variation is less than 1 % per hour. However, due to the software used in the present work, it is not possible to control each cell dynamically. For example, if cell 1 reaches stationary conditions it is not possible to start the next step of measuring protocol while the other cells stay in the conditioning process until they reach this goal. Instead, the measurement program must be defined before all test cells are built in. Therefore, in the future, the conditioning process must be extended to ensure that all cells reach a steady state.

Fig. 5c presents the low to high current density VI-curve of 20 mini cells. Apart from a few cells with conspicuous behavior, the majority of the cells achieve a performance that is comparable to the data from other measurements, such as a round robin test and measurements from other groups, also listed in this publication [25]. The cells that did not reach stationary conditions during the conditioning process (cells 21, 20, 18 and 16) exhibit an increased slope in the upper regime of the polarization curve. While the exact reasons for this remain unidentified, the increasing gradient with current density may indicate a mass transport limitation. However, contacting issues within the cell, which may intensify with increasing gas evolution, cannot be entirely ruled out. To address these uncertainties, further development of the test stand should explore whether dynamic measurement techniques can

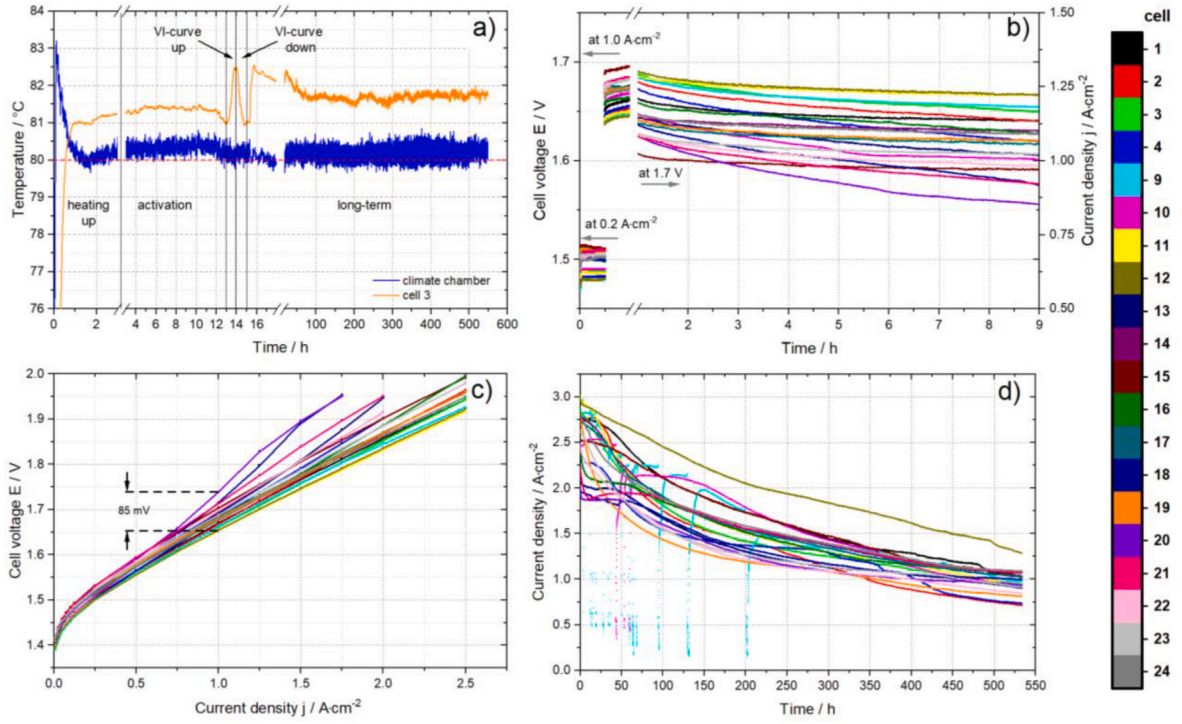

Fig. 5. – Measuring data of electrochemical cell-characterization (20 mini-cells): a) temperature inside the climate chamber and cell 3 versus absolute time; b) process of cell conditioning with first galvanostatic 0.2 A cm^{-2}, second galvanostatic 1.0 A cm^{-2} and third potentiostatic 1.7 V; c) VI-curve upwards with highlighted maximum spread between the curves at 1 A cm^{-2}; d) 530 h long-term operation at 2 V.

provide further insights.

Compared to the round-robin test, the spread between the curves at 1 A cm^{-2} is about ten times higher (85 mV with a standard deviation of 1.3 %). While five consecutive measurements were conducted in the same test cell during the round-robin test [25], this study employed 20 mini-cells simultaneously. Although the mini-cells and MEAs were expected to be similar, and inaccuracies within a batch of MEAs should be minimal, we anticipated a lower deviation in the results. It is presumed that the polishing process used to remove the ridge caused by laser cutting may have introduced variations in the morphology of the anodic PTLs. These inconsistencies, which might be detected visually as slight differences in surface appearance, likely contributed to the performance variations. Notably, four mini cells utilizing softer Ti-PTLs, which did not require post-manufacturing polishing, exhibited a standard deviation (0.1 % at 1 A cm^{-2}) comparable to the round-robin test. Therefore, this data may provide insights into the impact of PTL morphology on performance measurements.

Fig. 5d shows the plotted current densities of the cells at a voltage of constant 2 V over time. The cells 9 and 10 (light blue and violet) show conspicuous behavior during the measurements, as the current density is fluctuating until the first 200 h where current densities of more than 1.7 A cm^{-2} have been achieved. This phenomenon was observed in pre-measurements before, and it indicates an inadequate water supply. It was found, that if the inner diameter of the vertical anodic system is lower than 10 mm, at high current density and gas production water cannot reach the cell anymore and the current density decreases. In the setup of this work the inner diameter is sufficient but because of an error in cell manufacture a gap between flange and fitting was closed by a porous titanium ring. Initial experiments have shown that the gap has a significant effect on the rate of water depletion. Gas bubbles can accumulate until no water can reach the PTL. Closing this gap with a PTFE-ring and porous metal ring, respectively, reduces the observation of this process. Notwithstanding gas can absorb on the rough surface of the gap filler and form a barrier for water supply.

In agreement with the measuring results above this effect disappears with decreasing current density and thus decreasing gas production. A future improvement is to replace the fittings with a longer variant to receive a continuous, smooth tunnel. For the future, a revised cell design would be considered. The next generation will be planned with four screws to enable a better pressure distribution during the assembling process and the possibility to use a wider anodic water supply line with a diameter bigger than 10 mm to be sure to prevent water depletion at higher current densities. Also an analysis of the water with respect to a possible contamination with impurities that my affect the degradation should be performed when modifying the mini cell.

5. Conclusion

The multiple mini-cell test rig demonstrated in this work is a simple to set up, cost-effective, and space-efficient, and highly scalable alternative to traditional single-cell test stations. Its meticulous cell design and PTL preparation ensure high reproducibility, while its high-throughput screening capability significantly reduces measurement time and material costs. This is confirmed by the analysis of the components required for the system setup, which in the high throughput test station described here only ~1.42 (Table 1). This setup enables rapid evaluation of OER catalysts under realistic operating conditions and facilitates component testing at both the PTL and MEA levels. By increasing test capacity 24-fold compared to single-cell stations with consecutive measurements, this approach accelerates PEM electrolysis research and development, driving advancements in the field.

Future efforts will focus on further refining the mini-cell test rig to enhance its reliability and performance. One key area of improvement will be optimizing the water supply lines to ensure consistent flow and prevent potential blockages, thereby improving long-term stability. Additionally, advancing the cell design and PTL preparation methods will be essential to achieving even higher reproducibility and accuracy in test results. A critical step will be as well in scaling the design for industrial applications. It could be an option to derive a single cell setup from stack constructions. Another interesting option could be in

integrating automation and machine learning for predictive analysis and enhancing thermal and fluid management for long-term stability. Expanding operational conditions to include pressurized and dynamic load testing will further validate the test rigs robustness and industry applicability. Additionally, collaborations with industry partners will support commercial adaptation, bridging the gap between laboratory-scale research and full-scale electrolyzer development.

Through these advancements, the mini-cell test rig will evolve into a fully automated, scalable, and industry-ready platform, accelerating innovation in PEM electrolysis technology.

CRediT authorship contribution statement

Florian Berg: Data curation, Conceptualization. **Meital Shviro:** Writing – review & editing, Writing – original draft, Methodology, Investigation, Conceptualization. **Marcelo Carmo:** Writing – review & editing, Supervision, Project administration. **Nikolai Utsch:** Investigation, Data curation. **Martin Müller:** Writing – review & editing, Writing – original draft, Project administration.

Declaration of competing interest

The authors declare that they have no known competing financial interests or personal relationships that could have appeared to influence the work reported in this paper.

Acknowledgements

The authors are grateful for the great support from Norbert Commerscheidt, Stefanie Fischer, Daniel Holtz and Richard Wegner. The work was funded by the Deutsche Forschungsgemeinschaft (DFG, German Research Foundation) - 491111487.

References

[1] Barbir F. PEM electrolysis for production of hydrogen from renewable energy sources. Sol Energy 2005;78(5):661–9.
[2] Ayers K, et al. Perspectives on low-temperature electrolysis and potential for renewable hydrogen at scale. Annu Rev Chem Biomol Eng 2019;10:219–39.
[3] Buttler A, Spliethoff H. Current status of water electrolysis for energy storage, grid balancing and sector coupling via power-to-gas and power-to-liquids: a review. Renew Sustain Energy Rev 2018;82:2440–54.
[4] Carmo M, et al. A comprehensive review on PEM water electrolysis. Int J Hydrogen Energy 2013;38(12):4901–34.
[5] Ito H, et al. Experimental study on porous current collectors of PEM electrolyzers. Int J Hydrogen Energy 2012;37(9):7418–28.
[6] Rakousky C, et al. An analysis of degradation phenomena in polymer electrolyte membrane water electrolysis. J Power Sources 2016;326:120–8.
[7] Liu C, et al. Performance enhancement of PEM electrolyzers through iridium-coated titanium porous transport layers. Electrochem Commun 2018;97:96–9.
[8] Gago AS, et al. Protective coatings on stainless steel bipolar plates for proton exchange membrane (PEM) electrolysers. J Power Sources 2016;307:815–25.
[9] Ayers K, et al. PEM electrolysis, a forerunner for clean hydrogen. Electrochem Soc Interface 2021;30(4):67–71.
[10] Bernt M, et al. Current challenges in catalyst development for PEM water electrolyzers. Chem Ing Tech 2020;92(1–2):31–9.
[11] Borup RL, et al. Recent developments in catalyst-related PEM fuel cell durability. Curr Opin Electrochem 2020;21:192–200.
[12] Browne MP, et al. Oxygen evolution catalysts under proton exchange membrane conditions in a conventional three electrode cell vs. electrolyser device: a comparison study and a 3D-printed electrolyser for academic labs. J Mater Chem A 2021;9(14):9113–23.
[13] Fathi Tovini M, et al. The discrepancy in oxygen evolution reaction catalyst lifetime explained: RDE vs MEA - dynamicity within the catalyst layer matters. J Electrochem Soc 2021;168(1).
[14] Spöri C, et al. Accelerated degradation protocols for iridium-based oxygen evolving catalysts in water splitting devices. J Electrochem Soc 2021;168(3).
[15] Farchmin F. Development of large scale electrolysis systems: necessity and approach. 2016. p. 209–22.
[16] Babic U, et al. Critical review—identifying critical gaps for polymer electrolyte water electrolysis development. J Electrochem Soc 2017;164(4):F387–99.
[17] Rakousky C, et al. The stability challenge on the pathway to high-current-density polymer electrolyte membrane water electrolyzers. Electrochim Acta 2018;278:324–31.
[18] Feng Q, et al. A review of proton exchange membrane water electrolysis on degradation mechanisms and mitigation strategies. J Power Sources 2017;366:33–55.
[19] Lohoff AS, et al. Enabling high throughput screening of polymer electrolyte membrane (PEM) water electrolysis components via miniature test cells. J Electrochem Soc 2016;163(11):F3153–7.
[20] Li S, et al. Study on the aging of three typical rubber materials under high- and low-temperature cyclic environment. E-Polymers 2023;23(1).
[21] Barra G, et al. A comprehensive review on the thermal stability assessment of polymers and composites for aeronautics and space applications. Polymers 2023;15(18):3786.
[22] Burdzik A, et al. Homogeneity analysis of square meter-sized electrodes for PEM electrolysis and PEM fuel cells. J Coating Technol Res 2018;15(6):1423–32.
[23] Laube A, et al. PEM water electrolysis cells with catalyst coating by atomic layer deposition. Int J Hydrogen Energy 2021;46(79):38972–82.
[24] Scheepers F, et al. Temperature optimization for improving polymer electrolyte membrane-water electrolysis system efficiency. Appl Energy 2021;283:116270.
[25] Bender G, et al. Initial approaches in benchmarking and round robin testing for proton exchange membrane water electrolyzers. Int J Hydrogen Energy 2019;44(18):9174–87.